CANADIAN JOURNAL OF EXPLORATION GEOPHYSICS
VOL. 29, NO. 2 (DECEMBER 1993), P. 402-410

# WAVE PROPAGATION IN VISCOACOUSTIC HETEROGENEOUS MEDIA: A VELOCITY-PRESSURE FINITE-DIFFERENCE METHOD[1]

ANTONIOS VAFIDIS,[2] NANXUN DAI[3] AND ERNEST KANASEWICH[4]

## ABSTRACT

We present the particle velocity-pressure finite-difference method for modelling viscoacoustic wave propagation in heterogeneous media. In this method, the viscoacoustic modulus is approximated by a low-order rational function. Then, the convolution integral, present is the viscoacoustic constitutive relation, is transformed into a differential form. The equations of motion, the viscoacoustic constitutive relation and the additional differential equations form a first-order hyperbolic system. This system is solved by applying dimensional splitting and (2,4) finite-difference operators. Any desired variation of $Q$ or inverse attenuation with frequency may be used. The method appears to be a very efficient way of incorporating the quality factor $Q$ into finite-difference programs for viscoacoustic media.

As an example, viscoacoustic synthetic seismograms have been compared with field data from crosshole seismic experiments for monitoring steam injection projects in the Cold Lake area. These computer simulations not only describe the time delays due to the existence of the low-velocity steam zone but also explain the amplitude decrease of waves propagating through the anelastic media.

## INTRODUCTION

Considerable progress has been made during the past two decades on aspects of seismic attenuation. By seismic wave attenuation one means any irreversible energy losses other than spherical divergence, transmission losses and mode conversions which a seismic wave experiences as it propagates through a medium. Evidence from different experiments supports the fact that several physical mechanisms must contribute to seismic attenuation in rocks. The dramatic increase in attenuation due to the addition of trace amounts of water to a dry, porous rock has focussed attention on details of flow within fine cracks (Nur et al., 1980). Coulomb friction between grains yields attenuation which depends upon the amplitude of vibration. The motion of lattice dislocations within the solid gives the right dependence on frequency and the correct magnitude of attenuation in granite and makes this an attractive choice for the loss mechanism (Mason, 1969).

For seismic waves in the shallow crust, the attenuation is usually proportional to frequency. In principle, velocity must depend upon frequency in an attenuating medium. Several attempts have been made to find modifications of Hooke's law that would account for the effects of anelasticity. Attempts to account for the observed variation of the quality factor $Q$ with frequency can be divided into two groups: those invoking linear models and those invoking nonlinear models (Knopoff, 1964). Nonlinearity seems to have been largely ignored because of the mathematical difficulties associated with nonlinear models.

In perfect elasticity, strain is linearly proportional to stress and independent of the duration of the stress. When the stress is removed, the original form is recovered at once. In viscoelasticity, the strain under constant stress increases at a decreasing rate. When the stress is removed, there is an immediate recovery by the amount of the initial strain and the strain decreases further, ultimately tending to zero (Jeffreys, 1976). In Boltzmann's early theory (1876) to explain the nature of acoustic loss, the strain due to an applied stress is delayed by some sort of "memory" behaviour in the material. For a stress excitation which is a complicated function of time, the strain can be expressed as a convolution of the excitation with a creep function which expresses the delay.

It is difficult to incorporate attenuation into the time-domain computations of seismic wave fields because of the presence of a convolution integral which describes Boltzmann's superposition principle. Day and Minster (1984) attempted to use realistic attenuation laws in time-domain methods by applying a Padé approximation to the viscoelastic modulus. Then, the convolution integral which describes the stress-strain relation is transformed into a differential form. Carcione et al. (1988a, b) and Tal-Ezer et al. (1990) apply a similar approximation and solve numerically

[1]Presented at the C.S.E.G. National Convention, Calgary, Alberta, May 6, 1993. Manuscript received by the Editor July 10, 1993; revised manuscript received November 24, 1993.

[2]Technical University of Crete, Chania, Greece

[3]Presently, Department of Physics, University of Toronto, Toronto, Ontario M5S 1A7

[4]Seismology Laboratory, Department of Physics, University of Alberta, Edmonton, Alberta T6G 2J1

We would like to express our appreciation for financial support by the Alberta Oil Sands Technology and Research Authority (AOSTRA) and to ESSO Resources Canada Limited for providing the field data. Additional support was provided by the Natural Sciences and Engineering Research Council of Canada (NSERC).

the wave propagation problem using the pseudospectral method. In practice, the technique based on a Padé approximation gives valid results only for relatively short propagation paths. Emmerich and Korn (1987) proposed a method for incorporating attenuation in the time domain based on the rheological model of the generalized Maxwell body. The advantage of this technique is that the results are satisfactory for longer propagation paths and also strong attenuation.

In this paper, the viscoacoustic modulus which describes an arbitrary $Q$ law is approximated by the modulus of a generalized Maxwell body which is expressed as a rational function in the frequency domain. The advantage of the method we use is that a first-order hyperbolic system is formulated in the time domain and the particle velocity-pressure finite-difference method is applied to the viscoacoustic wave equation. A first-order system allows one to introduce lateral and vertical changes in the parameters as an input in the first-order algorithm. Finally, the results from the application of the method in a crosshole experiment are presented and compared to the real data.

## Problem Formulation

In a two-dimensional viscoacoustic heterogeneous medium, the equations of motion can be expressed in terms of the particle velocity components $v_x$, $v_z$ and the pressure $p$ as

$$\rho \frac{\partial v_x}{\partial t} = \frac{\partial p}{\partial x} \tag{1}$$

and

$$\rho \frac{\partial v_z}{\partial t} = \frac{\partial p}{\partial x}, \tag{2}$$

where $\rho$ is the density. The viscoacoustic constitutive relation is expressed by

$$p(t) = \int_{-\infty}^{t} K(t-\tau)\varepsilon(\tau)d\tau, \tag{3}$$

where $\varepsilon$ is the strain and $K$ is the viscoacoustic modulus that vanishes for negative time. The relationship between stress and strain given in (3) was first introduced by Boltzmann (1876). Equation (3) is not useful in forward modelling with finite-difference methods because the numerical integration of the strain history at each point of the medium and each time step would require an immense amount of computer memory.

In the frequency domain, equation (3) is formulated as

$$p(\omega) = K(\omega)\,\varepsilon(\omega), \tag{4}$$

where $K(\omega)$ is the complex viscoacoustic modulus. The modulus of the rheological model of the generalized Maxwell body (Figure 1) can be written in a rational function as

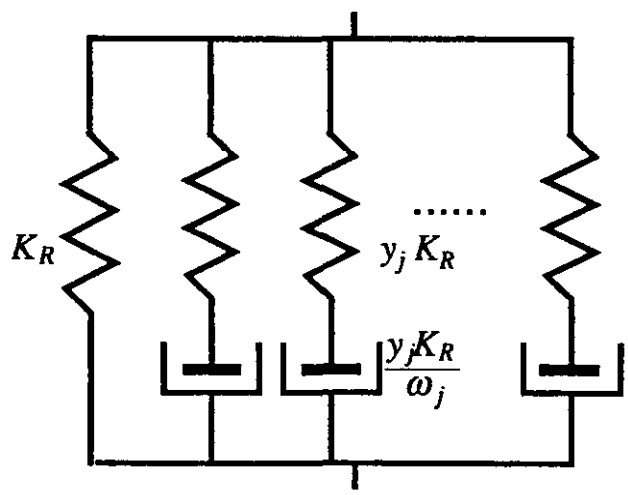


**Fig. 1.** Generalized Maxwell body with viscosities $\frac{y_j K_R}{\omega_j}$, elastic moduli $y_j K_R$ and an additional elastic element $K_R$.

$$K_n(\omega) = K_R\left(1 + \sum_{j=1}^{n} y_j \frac{i\omega}{i\omega + \omega_j}\right), \tag{5}$$

where

$$y_j = \alpha_j \frac{K_U - K_R}{K_R}$$

and $K_R$, $K_U$ are the relaxed and unrelaxed moduli respectively; $a_j$ are weighting factors with

$$\sum_{j=1}^{n} \alpha_j = 1.$$

Each term of the sum in equation (5) can be interpreted as a classical Maxwell body with viscosity $y_j/\omega_j$ and elastic modulus $y_j$ and the term $K_R$ represents an additional elastic element in the generalized Maxwell body (Figure 1). The quality factor $Q$ for the generalized Maxwell body is described by:

$$Q^{-1}(\omega) = \frac{\mathrm{Im}\left[K_n(\omega)\right]}{\mathrm{Re}\left[K_n(\omega)\right]} = \frac{K_U - K_R}{K_R} \frac{\sum_{j=1}^{n} \alpha_j \frac{\omega/\omega_j}{1+(\omega/\omega_j)^2}}{1 + \frac{K_\delta}{K_R}\sum_{j=1}^{n} \alpha_j \frac{(\omega/\omega_j)^2}{1+(\omega/\omega_j)^2}}. \tag{6}$$

For a given function $Q(\omega)$, a generalized Maxwell body model can be found as an approximation by determining the unknown parameters $y_j$ through a fitting procedure. Following Emmerich and Korn (1987), we utilize the values of $\tilde{Q}^{-1}(\omega)$ at certain discrete frequencies $\tilde{\omega}_l$ with $l = 1, 2, \ldots, L$ which are uniformly distributed on a logarithmic scale. Then, from equation (6), we obtain an overdetermined linear system:

$$\sum_{j=1}^{n} \frac{\tilde{\omega}_l\left[\tilde{\omega}_j - \omega_l \tilde{Q}^{-1}(\tilde{\omega}_l)\right]}{\omega_j^2 + \tilde{\omega}_l^2} y_j = \tilde{Q}^{-1}(\tilde{\omega}_l), \quad l = 1, 2, \ldots L, \quad (7)$$

which is solved for $y_j$ by applying a least-squares method. If we replace $K(\omega)$ in equation (4) with $K_n(\omega)$ in equation (5), then the constitutive relation becomes

$$p(\omega) = K_R \varepsilon(\omega) + \sum_{j=1}^{n} \eta_j(\omega), \quad (8)$$

where

$$\eta_j(\omega) = K_R y_j \frac{i\omega}{i\omega + \omega_j} \varepsilon(\omega). \quad (9)$$

The constitutive relation in the time domain can be expressed in a differential form. By inverse Fourier transforming and taking the time derivative, equations (8) and (9) become

$$\frac{\partial p}{\partial t} - \sum_{j=1}^{n} \frac{\partial \eta_j}{\partial t} = K_R \left( \frac{\partial v_x}{\partial x} + \frac{\partial v_z}{\partial z} \right) \quad (10)$$

and

$$\frac{\partial \eta_j}{\partial t} = y_j K_R \left( \frac{\partial v_x}{\partial x} + \frac{\partial v_z}{\partial z} \right) - \omega_j \eta_j, \quad j = 1, 2, \ldots n. \quad (11)$$

Equations (1), (2), (10) and (11) form a system which, in matrix form, can be written as

$$\frac{\partial \mathbf{u}}{\partial t} = \mathbf{A} \frac{\partial \mathbf{u}}{\partial x} + \mathbf{B} \frac{\partial \mathbf{u}}{\partial z} + \mathbf{C}\mathbf{u}. \quad (12)$$

Therefore, the convolution integral present in the constitutive relation (3) has been replaced by a set of first-order differential equations with a number of intermediate variables. By keeping the number of terms in (5) small, this method of incorporating attenuation into time-domain computations of the seismic wave field is quite tractable.

If we choose $n = 5$, then the vector of unknowns of system (12) is

$$\mathbf{u} = \begin{bmatrix} v_x \\ v_z \\ p \\ \eta_1 \\ \eta_2 \\ \eta_3 \\ \eta_4 \\ \eta_5 \end{bmatrix} \quad (13)$$

and the matrices become

$$\mathbf{A} = \begin{bmatrix} 0 & 0 & \rho^{-1} & 0 & 0 & 0 & 0 & 0 \\ 0 & 0 & 0 & 0 & 0 & 0 & 0 & 0 \\ A_{31} & 0 & 0 & 0 & 0 & 0 & 0 & 0 \\ y_1 K_R & 0 & 0 & 0 & 0 & 0 & 0 & 0 \\ y_2 K_R & 0 & 0 & 0 & 0 & 0 & 0 & 0 \\ y_3 K_R & 0 & 0 & 0 & 0 & 0 & 0 & 0 \\ y_4 K_R & 0 & 0 & 0 & 0 & 0 & 0 & 0 \\ y_5 K_R & 0 & 0 & 0 & 0 & 0 & 0 & 0 \end{bmatrix} \quad (14)$$

$$\mathbf{B} = \begin{bmatrix} 0 & 0 & 0 & 0 & 0 & 0 & 0 & 0 \\ 0 & 0 & \rho^{-1} & 0 & 0 & 0 & 0 & 0 \\ 0 & B_{32} & 0 & 0 & 0 & 0 & 0 & 0 \\ 0 & y_1 K_R & 0 & 0 & 0 & 0 & 0 & 0 \\ 0 & y_2 K_R & 0 & 0 & 0 & 0 & 0 & 0 \\ 0 & y_3 K_R & 0 & 0 & 0 & 0 & 0 & 0 \\ 0 & y_4 K_R & 0 & 0 & 0 & 0 & 0 & 0 \\ 0 & y_5 K_R & 0 & 0 & 0 & 0 & 0 & 0 \end{bmatrix} \quad (15)$$

and

$$\mathbf{C} = \begin{bmatrix} 0 & 0 & 0 & 0 & 0 & 0 & 0 & 0 \\ 0 & 0 & 0 & 0 & 0 & 0 & 0 & 0 \\ 0 & 0 & 0 & -\omega_1 & -\omega_2 & -\omega_3 & -\omega_4 & -\omega_5 \\ 0 & 0 & 0 & -\omega_1 & 0 & 0 & 0 & 0 \\ 0 & 0 & 0 & 0 & -\omega_2 & 0 & 0 & 0 \\ 0 & 0 & 0 & 0 & 0 & -\omega_3 & 0 & 0 \\ 0 & 0 & 0 & 0 & 0 & 0 & -\omega_4 & 0 \\ 0 & 0 & 0 & 0 & 0 & 0 & 0 & -\omega_5 \end{bmatrix} \quad (16)$$

where

$$A_{31} = B_{32} = -K_R + K_R \sum_{j=1}^{5} y_j = K_U. \quad (17)$$

The matrices **A** and **B** have the same eigenvalues:

$$(\lambda_1, \lambda_2, \lambda_3, \lambda_4, \lambda_5, \lambda_6, \lambda_7, \lambda_8) = (-v, 0, 0, 0, 0, 0, 0, v), \quad (18)$$

where $v = \sqrt{K_U / \rho}$ is the high-frequency limit velocity of wave propagation. Since the eigenvalues of **A** and **B** are real and their eigenvectors are linearly independent, system (12) is hyperbolic. This first-order system is free of spatial derivatives of the physical parameters which are present in the second-order wave equations for heterogeneous media. Consequently, the numerical approximation of the spatial derivatives of the physical parameters is not required in the particle velocity-pressure finite-difference method. Numerical approximation of these derivatives may sometimes result in large errors especially at the location close to interfaces where the physical parameters change quickly. This source of error is not present in the above formulation of viscoacoustic wave equations for heterogeneous media.

The first-order system (12) is solved numerically for $t > 0$, subject to the initial condition $\mathbf{u}(x, z, t = 0)$, by applying the concept of dimensional splitting (Strang, 1968). A MacCormack-type finite-difference operator is then employed to solve the differential system alternately in the $x$ and $z$ directions. The fully vectorized finite-difference algorithm is second-order accurate in time and fourth-order in space (Vafidis et al., 1992; Dai, 1993). Since all the nonzero elements of **A** and **B** in (12) are in the first three columns, the spatial difference operators are applied only to the first three elements of the vector **u**. Therefore, increasing $n$, the number of the terms in (5) will require more computer memory, but it will not increase significantly the computational time. On a Convex 210, the CPU time is approximately 90 minutes for a 500 x 480 model and 1500 time steps when $n = 9$. An absorbing boundary technique (Dai, 1993) is incorporated in order to reduce the amplitudes of the artificial reflections from the margins of the computational region.

## Numerical Solution

In most seismic applications, the quality factor $Q$ is normally assumed to be frequency-independent or nearly frequency-independent. To test the quality of the generalized Maxwell body approximation, we have computed $Q(\omega)$ for $n = 5$ and $n = 9$ from (6) and compared them to the exact values for a constant $Q$ law over a range of frequencies from 0 to 250 Hz and $Q = 30$ (Figure 2). The approximation of $Q$ is very good for $n = 9$.

In a viscoacoustic homogeneous medium, the solution for particle velocity of the one-dimensional wave equation can be expressed as

$$v_x(x,t) = e^{-\alpha(\omega)x} e^{i[\omega t - x/V(\omega)]}, \tag{19}$$

where $\alpha(\omega)$ is the attenuation coefficient and $V(\omega)$ is the phase velocity given by

$$\alpha(\omega) = -\omega \operatorname{Im}\left[\left(\frac{K(\omega)}{\rho}\right)\right]^{-1/2} \tag{20}$$

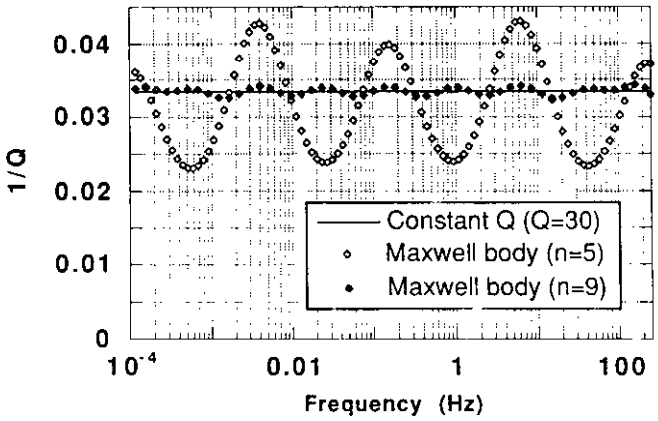


**Fig. 2.** Exact values (solid line) and generalized Maxwell body approximations for $n = 5$ (open diamonds) and $n = 9$ (solid diamonds) of the inverse $Q$ for a constant $Q$ model.

$$V(\omega) = \frac{1}{\operatorname{Re}\left[\left(\frac{K(\omega)}{\rho}\right)\right]^{-1/2}}. \tag{21}$$

For a constant $Q$ law, the modulus $K(\omega)$ is given by (Kjartansson, 1979):

$$K(\omega) = |K(\omega_o)| \left(\frac{i\omega}{\omega_o}\right)^{\frac{2}{\pi}\tan^{-1}(Q^{-1})}, \tag{22}$$

while the phase velocity $V(\omega)$ and the attenuation coefficient $\alpha(\omega)$ are described by

$$V(\omega) = \left(\frac{K(\omega_o)}{\rho}\right)^{1/2} \frac{1}{\cos\left[\frac{1}{2}\tan^{-1}(Q^{-1})\right]} \left|\frac{\omega}{\omega_o}\right|^{\frac{1}{\pi}\tan^{-1}(Q^{-1})} \tag{23}$$

and

$$\alpha(\omega) = \frac{\omega}{V(\omega)} \tan\left[\frac{1}{2}\tan^{-1}(Q^{-1})\right], \tag{24}$$

where $\omega_o$ denotes the fundamental angular frequency.

Numerical computations of $K_n(\omega)$ and $V_n(\omega)$ with the generalized Maxwell body approach for $n = 5$ and $n = 9$ are shown in Figures 3 and 4, for $Q = 30$ and V = 2550 m/s at $f_o = 35$ Hz. The exact values of $K(\omega)$ and $V(\omega)$ are calculated from (22) and (23). The approximation to the real part of $K(\omega)$ is good even for $n = 5$.

The impulse response is of particular interest, since the waveform can be obtained by simply convolving the source excitation with the impulse response. The amplitude spectrum of the impulse response is obtained by omitting the $i\omega t$ term in equation (19). Figure 5a shows the amplitude spectrum of the impulse response at a distance of 500 m from the shot location for a constant $Q$ model and its generalized Maxwell body approximations for $n = 5$ and $n = 9$. Figure 5b shows the pulse shape for a source whose excitation is equal to the second derivative of the Gaussian function with a dominant frequency of 35 Hz and its generalized Maxwell body approximations for $n = 5$ and $n = 9$. The approximations to the pulse shape and to the amplitude spectrum of the impulse response are very good for $n = 9$.

## Field Example

The bitumen from the oil sands is normally recovered by enhanced oil recovery (EOR) operations. Many of these operations involve steam injection to make the oil mobile. From the viewpoint of the reservoir engineer, it is important to monitor the growth of the steam fronts and to assess the changes occurring in the reservoir as a result of the steam stimulation. In particular, a knowledge of the size, position and physical state of the heated zone around the injection well is desired in the development of efficient heavy oil

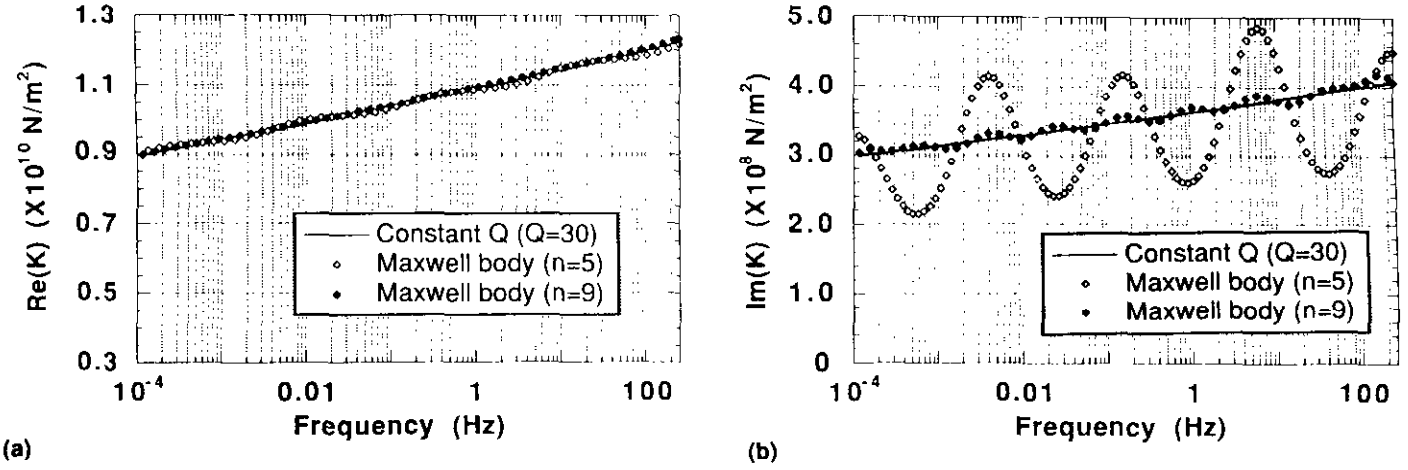


**Fig. 3.** Exact values (solid line) and generalized Maxwell body approximations for $n = 5$ (open diamonds) and $n = 9$ (solid diamonds) of the real **(a)** and the imaginary **(b)** parts of the complex modulus for a constant $Q$ model.

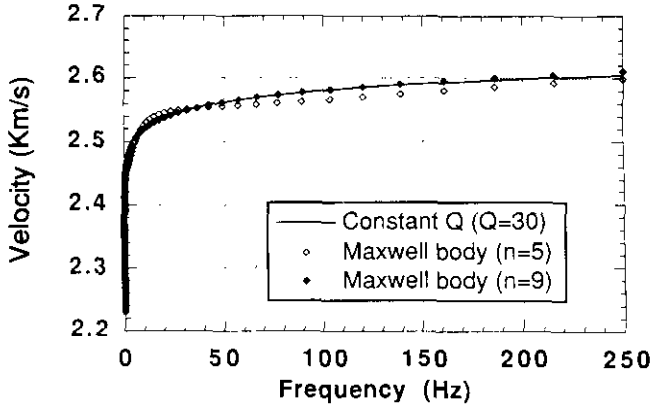


**Fig. 4.** Exact values (solid line) and generalized Maxwell body approximations for $n = 5$ (open diamonds) and $n = 9$ (solid diamonds) of the velocity for a constant $Q$ model.

extraction techniques. Invasive techniques, such as drilling observation wells, are expensive and limited in spatial resolution. Noninvasive or remote sensing geophysical techniques, especially the seismic method, have proven to be successful tools in delineating information about the heated zone.

Esso Resources Canada Limited carried out crosshole seismic experiments in the Cold Lake, Alberta area to monitor the steam injection process. The geometry of an initial crosshole experiment and the model with a steam heated zone are illustrated in Figure 6. The source well and the receiver well are separated by 200 m. An explosive source (100 grams of Primacord charge) located at a depth of 440 m within the source well has generated waves which contain frequencies up to 500 Hz. A well-locking vertical component seismometer was used for recording and was positioned at various depths between 372 m and 462 m within the receiver well. The data were recorded at a rate of 1000 samples/s.

Steam was injected from a well located half way between the receiver and source wells into the Clearwater (CLGW) Formation in order to mobilize the heavy oils. The velocity model is derived from well-log data (Kanasewich, 1983; Figure 6b). The top and bottom boundaries of the Clearwater are at depths of 415 m and 465 m, respectively. The top boundary is marked by the impermeable Grand Rapids (GR) shale formation which prevents the steam from escaping upwards. Two concentric ellipses, which are truncated at the top by a plane interface, are used to model the heated zone. In the inner zone the velocity is reduced by 25%. The outer zone is the transition zone where the velocity increases linearly from the velocity of the inner zone to its normal value for the Clearwater layer.

The field experiment was conducted twice; the first time was before steam injection and the second was after injecting steam at a pressure of 10 MPa for 48 days. The first 147 ms of the *before* and *after* steam injection seismograms are shown in Figure 7. Delays of up to 2 ms in the first arrivals are measured after steam injection at receivers 6 to 10. Moreover, the amplitudes on traces 6 to 9 from the two experiments are significantly lower in the after injection traces. Reflections from layers below and above the Clearwater are difficult to identify in the records. Macrides and Kanasewich (1987) studied this data set and, based on evidence from theoretical and experimental studies (Nur et al., 1980; Tosaya et al., 1984), modelled it with rays and a *P*-wave velocity drop of 20% within the steam zone. *P-SV* computer simulations using a finite-difference method were carried out by Vafidis and Kanasewich (1991) and provided insight into the later arrivals which correspond to converted phases. Macrides and Kanasewich (1987) also studied the amplitudes and the power spectra of the real data and they reported that in the steam zone $Q = 10$, while in the Clearwater Formation $Q = 30$. The decrease of $Q$ within the steam zone is mostly caused by the heated bitumen and steam condensate as well as by the microcracks created by the injection of highly pressurized steam (Macrides and Kanasewich, 1987). In order to verify the validity of these interpretation points, we carried out realistic simulations of wave propagation with time step equal to 0.05 ms and grid spacing equal to 0.5 m. The source excitation is a Gaussian function with a dominant frequency of 400 Hz.

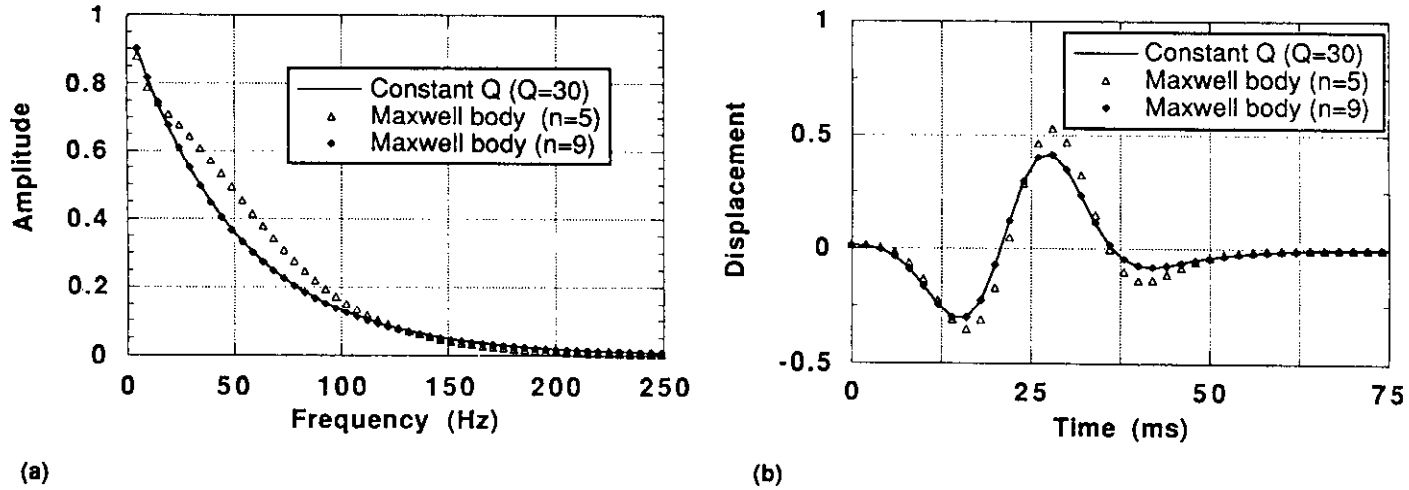


**Fig. 5. (a)** Exact values (solid line) and generalized Maxwell body approximations for $n = 5$ (open triangles) and $n = 9$ (solid diamonds) of the amplitude spectrum of impulse response for a constant $Q$ model. **(b)** Comparison of pulse shapes of the exact solution (solid line) and the generalized Maxwell body approximation for $n = 5$ (open triangles) and $n = 9$ (solid diamonds). The receiver is located at a distance $x = 500$ m from the source in the constant $Q$ model. The source excitation is the second derivative of Gaussian function with a dominant frequency of 35 Hz.

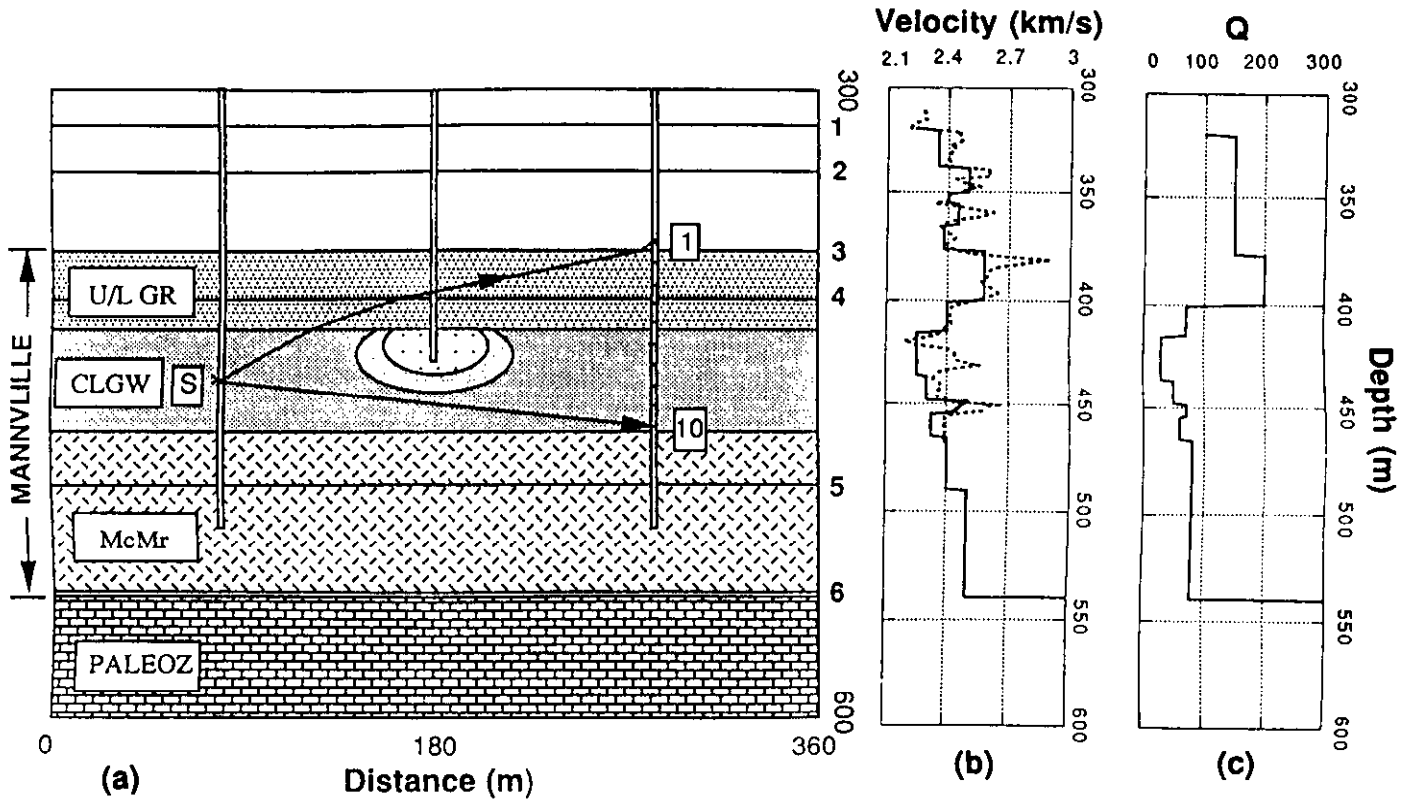


**Fig. 6.** Model for a seismic crosshole experiment **(a)** based on well-log data **(b)**. The quality factors $Q$ of each layer are given in **(c)**. The quality factor in the inner and outer zones of the steam heated region are 10 and 20, respectively.

We employed the acoustic wave equation in the initial computer simulation. The vertical component synthetic seismograms (Figure 8) contain quite high frequencies. We observe the expected time delays of the first arrivals up to 2 ms on traces 6 to 10. The amplitudes of the reflections from interfaces 6 and 4 are too high compared to the real data. In the after injection traces, the amplitudes of the reflections from interfaces 4 and 5 are less than the ones in the before steam traces. However, they are still higher than the ones in Figure 7, especially on traces 6 and 7.

Viscoacoustic modelling is then carried out for the same model geometry and for quality factors described in Figure 6c. The quality factors $Q$ in the Clearwater layer, the inner steam zone, and the transition zone are 30, 10 and 20, respectively (Macrides and Kanasewich, 1987). The generalized Maxwell body approximation with $n = 9$ has been

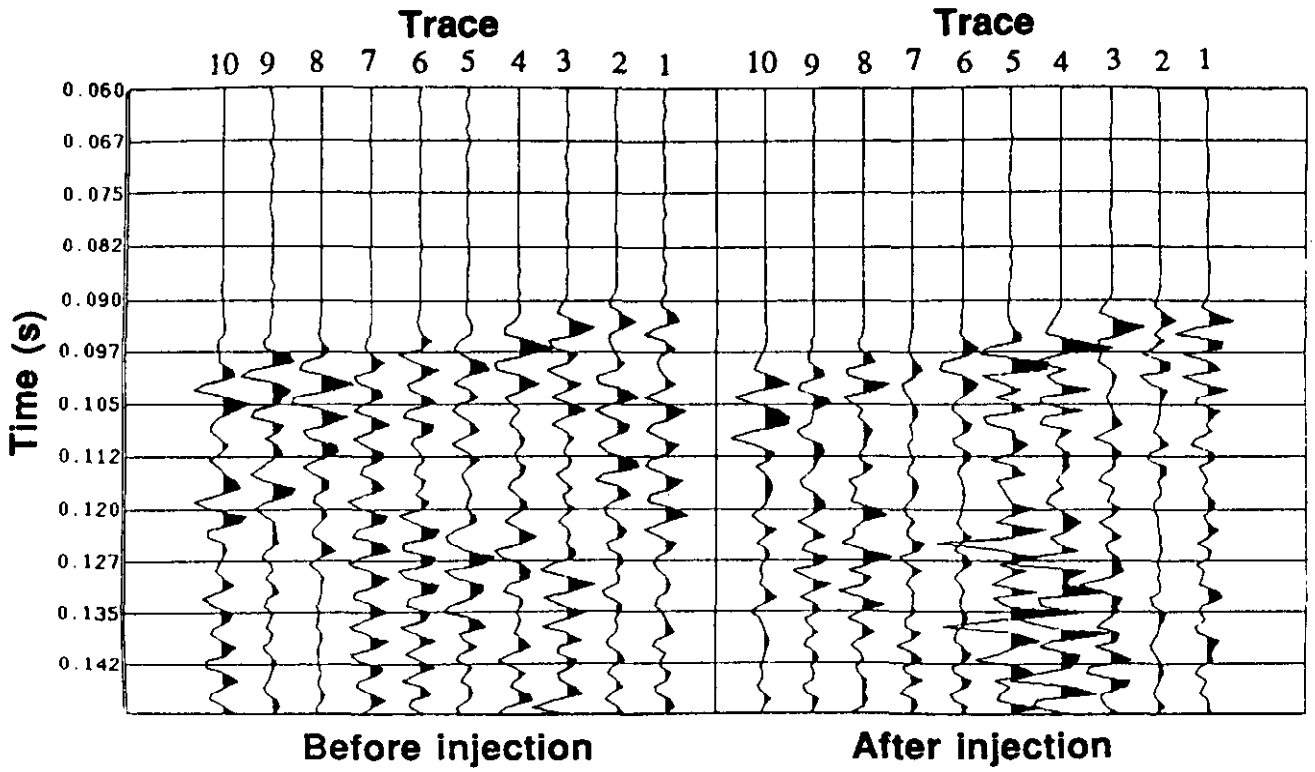


**Fig. 7.** Crosshole seismic experiment before and after steam injection.

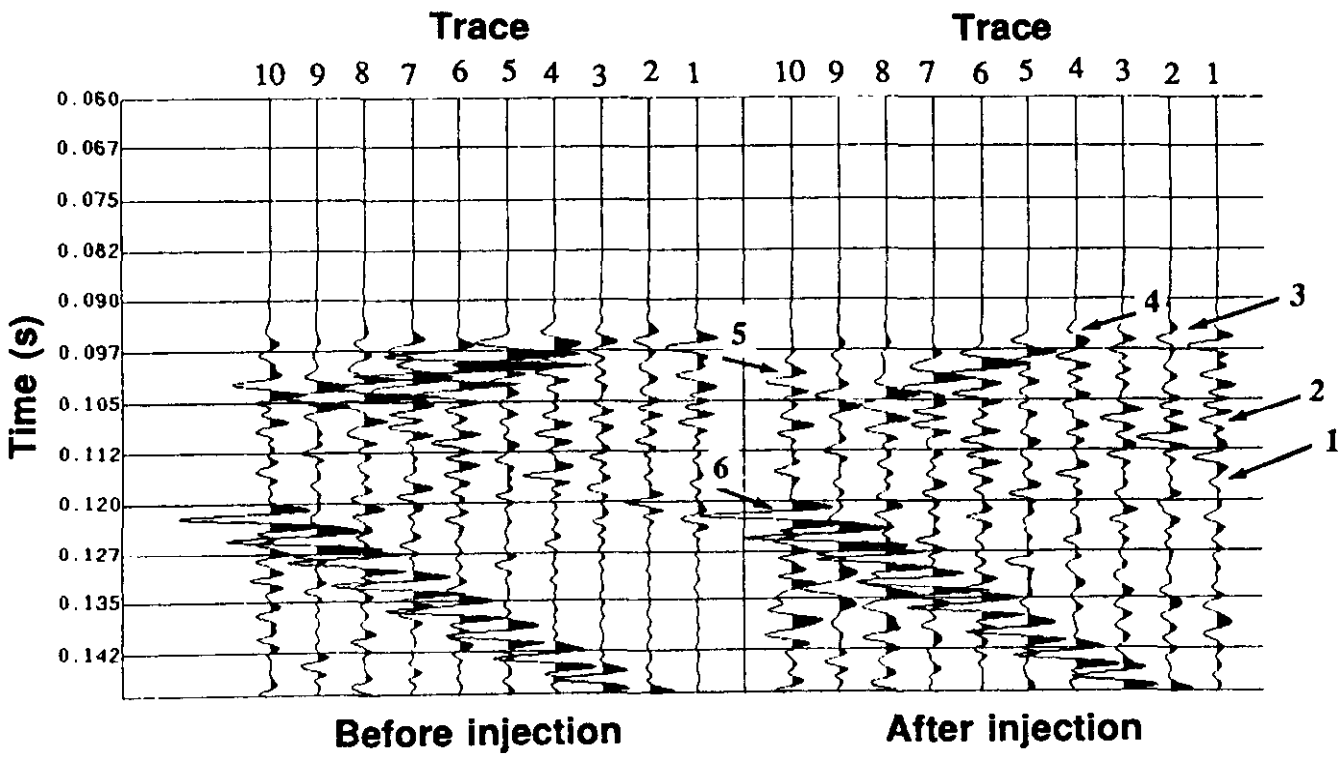


**Fig. 8.** Synthetic seismograms from acoustic modelling of the crosshole seismic experiment before and after steam injection. The indices of the reflection events refer to the reflectors (Figure 6a).

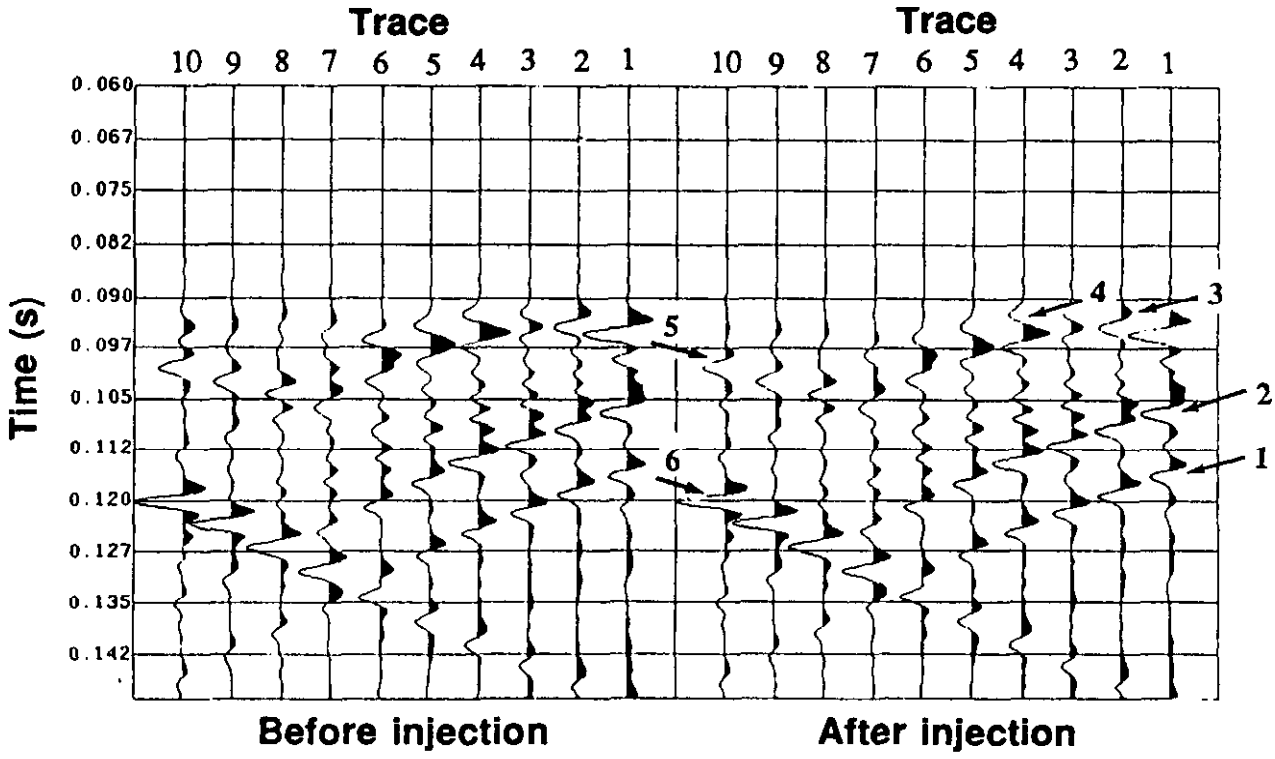


**Fig. 9.** Synthetic seismograms from viscoacoustic modelling of the crosshole seismic experiment before and after steam injection.

employed and the viscoacoustic moduli are determined by a least-squares fitting procedure in a frequency range from 0 to 800 Hz.

The synthetic seismograms from viscoacoustic modelling before and after steam injection (Figure 9) are somewhat but not perfectly compatible with the real data. At this stage the modelling was carried out to obtain a reasonable fit with direct first arrivals. Little consideration was given to reflections from the top of Paleozoic (event 6) or other layers remote from the injection level. The amplitudes on the after injection traces are less than the amplitudes on the before injection traces at receivers 6 to 9. Amplitude delays can be observed for reflections travelling through the Clearwater layer. Although this model by no means describes the complexity of the real data, the realistic finite-difference simulations with attenuation assist in the interpretation of the real data.

## Conclusion

Attenuation has been incorporated in the particle velocity-pressure finite-difference method by expressing the convolution integral in the viscoacoustic constitutive relation, in a differential form. The equations of motion, the viscoacoustic constitutive relation, and the additional differential equations form a first-order hyperbolic system which describes the wave motion in a heterogeneous viscoacoustic medium. This system is solved by applying a dimensional splitting technique and the MacCormack finite-difference operators which are second-order accurate in time and fourth-order accurate in space.

Viscoacoustic synthetic seismograms have been compared with field data from crosshole seismic experiments for monitoring steam injection projects in the Cold Lake area as well as with synthetic seismograms from acoustic modelling. The viscoacoustic modelling produces synthetic seismograms which are more compatible with the field measurements in terms of the frequency content. The simulations assist in interpreting the field data by establishing the relationship between the features of the seismic sections, such as the arrival time and the amplitude of reflected waves, and the physical parameters, such as the velocity and the quality factor of the formations.

## References

Boltzmann, L., 1876, Zur Theorie der elastiche Nachwirkung: Ann. Phys. Chem. Erqanzung **7**, 24-654.

Carcione, J.M., Kosloff, D. and Kosloff, R., 1988a, Wave propagation simulation in a linear viscoelastic medium: Geophys. J. Roy. Astr. Soc. **95**, 393-407.

_____, _____ and _____, 1988b, Wave propagation simulation in a linear viscoacoustic medium: Geophysics **53**, 769-777.

Dai, N., 1993, Finite difference simulation and imaging of seismic waves in complex media: Ph.D. thesis, Univ. of Alberta.

Day, S.M. and Minster, J.B., 1984, Numerical simulation of attenuated wavefields using Padé approximate method: Geophys. J. Roy. Astr. Soc. **78**, 105-118.

Emmerich, H. and Korn, M., 1987, Incorporation of attenuation into time domain computations of seismic wave fields: Geophysics **52**, 1252-1264.

Jeffreys, H., 1976, The earth: Cambridge Univ. Press.

Kanasewich, E.R., 1983, Cold Lake seismicity project: Rep. No. 3, Dept. of Physics, Univ. of Alberta.

Kjartansson, E., 1979, Constant $Q$-wave propagation and attenuation: J. Geophys. Res. **84**, 4737-4748.

Knopoff, L., 1964, $Q$: Rev. Geophys. **2**, 625-660.

Macrides, C.G. and Kanasewich, E.R., 1987, Seismic attenuation and Poisson's ratio in oil sands from crosshole measurements: J. Can. Soc. Expl. Geophys. **23**, 46-55.

Mason, W.R., 1969, Internal friction mechanism that produces an attenuation in the Earth's crust proportional to frequency: J. Geophys. Res. **74**, 4963-4966.

Nur, A., Walls, J.D., Winkler, K. and De Vilbiss, J., 1980, Effects of fluid saturation on waves in porous rock and relations to hydraulic permeability: J. Soc. Petr. Eng. **24**, 450-458.

Strang, G., 1968, On the construction and comparison of difference schemes: J. Soc. Ind. Appl. Math., Num. Anal. **5**, 506-517.

Tal-Ezer, H., Carcione, J.M. and Kosloff, D., 1990, An accurate and efficient scheme for wave propagation in linear viscoelastic media: Geophysics **55**, 1366-1379.

Tosaya, C.A., Nur, A.M. and Da Prat, G., 1984, Monitoring of thermal EOR fronts by seismic methods: western energy frontiers: Proc. Soc. Petr. Eng. **54**, 179-186.

Vafidis, A. and Kanasewich, E.R., 1991, Modelling crosshole seismic data in steam injection problems with finite differences: Can. J. Expl. Geophys. **27**, 23-33.

_____, Abramovici, F. and Kanasewich, E.R., 1992, Elastic wave propagation using fully vectorized high order finite differences: Geophysics **57**, 218-232.